THE EFFECT OF TENSILE STRENGTH IN THE ARCTIC ICE PACK

Mark A. Hopkins

US Army Cold Regions Research and Engineering Laboratory
Hanover, NH, USA
Mark.A.Hopkins@erdc.usace.army.mil

Abstract The ice pack covering northern seas is composed of an aggregate of thick ridged and rafted ice, undeformed ice, and open water. Existing ice-ocean models of the Arctic ice pack are large-scale continuum models that use a plastic yield surface to characterize the constitutive behavior of the pack. An alternative approach, which captures far more detail, is to explicitly model the ice parcels that make up the ice pack. To this end a granular model of the central Arctic ice pack has been developed. In the granular model each floe has its own ice thickness distribution. Deformation causes leads to open or ridges to form between floes. The granular sea ice model was used to simulate a range of deformation states from uniform convergence to uniform divergence Two sets of simulations were performed. In the first set the joints between neighboring floes were unfrozen and hence unable to support tensile forces, while in the second set the joints were frozen. Stresses in the simulations were calculated in three ways and compared. Yield surfaces constructed from the results of the simulations clearly demonstrate the effects of the tensile strength between floes. The difference in the yield curves is shown to be related to a qualitative difference in the deformation patterns in the model pack. Lastly the discussion looks at the differences between the global stress state in the model ice pack and the stress state in the individual floes.

1. Introduction

The large-scale processes and properties of the Arctic ice pack depend on the granular nature of the pack, particularly on the size and distribution of thin lead ice, open water, and multi-year floes. Thin ice and open water determine the strength of the pack and the rate of heat exchange between atmosphere and ocean necessary in global climate models, single-column models, and basin-scale ice-ocean models.

A granular model of the central Arctic ice pack was developed by *Hopkins* [1996] that embodied the granularity of the ice pack by explicitly considering individual multiyear floes in a matrix of first-year ice parcels. Thicknesses were assigned to each parcel from an assumed thickness distribution. Simulations were performed with the model to determine the plastic

J.P. Dempsey and H.H. Shen (eds.),
IUTAM Symposium on Scaling Laws in Ice Mechanics and Ice Dynamics,
373-386. ©Kluwer Academic Publishers. Printed in the Netherlands.

yield surface relating stress and deformation, the partition of energy dissipation between ridging and sliding between ice parcels, and the changes to the thickness distribution. However, this model was unsuitable for long duration simulations for two reasons. First, the time step was very small (≈0.02 s) due to the relatively low mass and high modulus of the first-year ice parcels. Second, with continuing deformation partially destroying parcels and creating open water to form new parcels, the level of detail in the model quickly became unmanageable.

This work uses a new granular model of the Arctic ice pack. Like the previous model this model also consists of thousands of discrete polygonal floes. However, small parcels of thin, first-year ice are not explicitly modeled. Instead the interior of each floe has its own thickness distribution. When the floe interacts with a neighbor the thinnest ice in each floe's thickness distribution is consumed. The advantages of this approach directly address the two shortcomings of the older model. First, the time step is much larger (≈1 s) because the mass of the floes is large. Second, the level of detail that accompanies deformation is greatly reduced by treating the interior of each floe as a continuum with its own thickness distribution, rather than trying to explicitly treat each small parcel of thin ice created by deformation.

This new granular sea ice model is used to examine the effects of the tensile strength of the joints between neighboring floes. The tensile strength between floes is shown to have a profound effect on the yield surface that is used to characterize pack ice constitutive behavior in basin scale sea ice models. The yield surface is determined by varying the deformation state in the model pack by degrees from uniform divergence through uniform convergence. The steady-state stresses calculated during each simulation are plotted on principal stress axes to define the yield surface. Two sets of simulations are performed. In the first set, the floes in the model pack are not frozen together, that is, the joints between neighboring floes do not support tensile forces. The stresses from this set of simulations form a perfect tear drop yield surface similar to the one found by *Hopkins* [1996]. In the second set, the floes are frozen together and able to support tensile forces. The stresses from this set of simulations form a Coulomb yield surface with a compressive cap [see *Coon et al*., 1998]. A detailed look at the deformation that occurs within the model pack shows that in the first unfrozen case the deformation is uniformly distributed over the entire domain, while in the frozen case the deformation is concentrated along the boundaries of large aggregates. This type of aggregate deformation has been found in Beaufort Sea SAR ice motion data by *Overland, et al.* [1998].

2. Granular Sea Ice Model

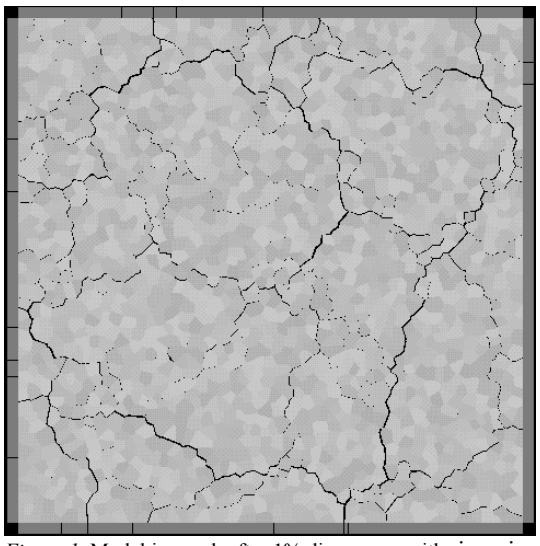

Figure 1. Model ice pack after 1% divergence with $\dot{e}_1 = \dot{e}_2$. The model pack is 90 × 90 km. The floes were initially frozen together. The shades of gray show the individual floes. The dark lines crossing the interior are leads.

The granular sea ice model consists of thousands of discrete polygonal floes. The interior of each floe is a continuum with its own thickness distribution. The model domain is a rectangular area that can be placed at an arbitrary location in the Arctic basin. The initial configuration of the model ice pack, constructed by dividing a rectangular control area into a Voronoi tessellation, is shown in Figure 1. The dark band around the model domain in Figure 1 is composed of boundary floes. The boundary floe motions can be kinematically defined by ice motion data from large-scale model output or SAR velocity products. In the interior of the domain the floes can be driven by wind stress derived from daily average geostrophic wind fields or by measured wind stress and by Coriolis forces. Floe motion is retarded by water drag. The floes can freeze together so that the joints between floes can support tensile as well as compressive forces. Deformation causes the floes in the interior of the domain to be pushed together to form pressure ridges and pulled apart to form leads. When a pair of neighboring floes are pushed together the polygons defining the shape of each floe intersect. The geometric algorithm used to define the intersection of the floe polygons is described by *Hopkins* [1996]. The intersection area is interpreted as thin ice destroyed by ridging. The thinnest ice in the thickness distribution belonging to each floe is ridged.

Ridging forces at points of contact between converging floes are determined from the results of computer simulations of the pressure ridging process [*Hopkins*, 1998]. The ridging force (per meter of ridge length) as a function of lead ice thickness h and the extent or length of lead ice L that is

pushed into the ridge was $F=7300h^{3/2}L^{1/2}$ during stage 1 (the period of sail growth) and $F=95400h^{3/2}$ during stage 2 (when the sail has reached its maximum size).

In the simulations described in this paper the floes in the 90×90 km model pack are initially frozen together. That is, the joints between neighboring floes are capable of supporting tensile strength. A crack is initiated in a joint when the stress at either end of the joint exceeds the specified tensile strength σ_t in tension or a compressive strength criteria based on unconfined buckling strength [*Kovacs and Sodhi*, 1980]. Once initiated the crack travels at a constant speed until the joint is broken. In this study the model pack is driven by a uniform deformation field. Deformation of the domain is accomplished by distorting the domain by specifying the principal strain rates $\dot{e}_{xx}$ (∂u/∂x) and $\dot{e}_{yy}$ (∂v/∂y), which are held constant for the duration of each simulation. The equation describing the floe motion is

$$\bar{x}^{n+1} = \bar{x}^{n} + \Delta t(\bar{v} + \bar{x} \cdot \tilde{e}) \tag{1}$$

where the superscript n denotes the current time step, Δt is the length of the time step, and $\tilde{e}$ is the strain rate tensor. The velocity $\vec{v}$ is the fluctuating component about the prescribed mean motion. Although the mean motion of the ice floes is constrained, individual floes are free to move in response to applied forces. The boundary floes, whose fluctuating velocity $\vec{v} = 0$, do not respond to applied forces. This simulation technique was developed by *Cundall and Strack* [1979]. The technique was used by *Hopkins* [1996] with periodic boundaries in an earlier granular simulation of the ice pack. In this study the ocean is stationary. The model pack in Figure 1 was subjected to uniformly divergent deformation at strain rates of $\dot{e}_{xx}=\dot{e}_{yy}= 1\text{x}10^{-6}\text{s}^{-1}$. The duration of the simulation was 5000 s. The dark lines crossing the pack are leads. The figure shows that, although the applied deformation field is uniform, the response is not. Water drag is applied with a linear drag coefficient to the fluctuating velocities.

3. Three Methods of Calculating Stress

Stress in the model pack was calculated in three different ways. The first method was to sum forces at each boundary and divide by the length of the boundary. I call this the boundary stress method. The second method was to sum interior forces at contacts between neighboring floes, an approach developed by *Cundall and Strack* [1979]. The equation for this version of the stress is

$$\sigma_{ij} = \frac{\Delta t}{TA} \sum r_i F_j \qquad (2)$$

where r_i is the vector connecting the center of two floes, F_j is the force between them, T is the sampling interval, and A is the area of the model ice pack. The summation is over every contact at each time step during the sampling interval. I call this the internal stress method.

The third method is based on a linear elastic boundary element model [*Brebbia and Dominguez*, 1992]. One hundred floes in the model ice pack were chosen at random. At 10 s intervals the contact forces and their locations on the floes were stored. After the simulation the floe boundaries were divided into quadratic boundary elements with nodes at each vertex and at the center of each side. D'Alembert forces were applied to the nodes. The contact forces on the floe and the d'Alembert forces were divided amongst the nodes such that the sum of the x and y forces and the torque on the floe were zero. Nodal pressures were calculated from the nodal forces. The stresses at the center of the floe were calculated using the boundary element program of *Brebbia and Dominguez* [1992]. That the three methods give similar results is shown in Figure 2. The figure compares the stresses σ_{xx} and σ_{yy} calculated using the 3 approachs described above. Compressive stresses are negative. The results are from a simulation in which the principal strains $\dot{e}_{xx} = -\dot{e}_{yy} = -10^{-6}$ s^{-1} (ie. pure shear). In this simulation the floes were initially frozen together. The initial rapid rise and fall in the magnitudes of both stresses is caused by the rapid loading and breaking of some of the initially frozen joints in the model pack. Approximately 3000 of the initial 5000 frozen joints remain frozen at the end of the simulation. Interest-

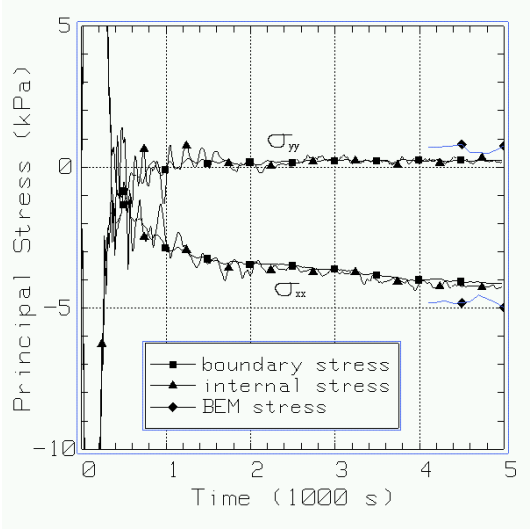

Figure 2. Comparison of the stresses σ_{xx} and σ_{yy} calculated using 3 different approachs from a simulation in which the principal strains $\dot{e}_{xx} = -\dot{e}_{yy} = 10^{-6}$ s^{-1} (ie. pure shear). In this simulation the floes were initially frozen together.

ingly, this result varied little over the whole range of deformation states. After the initial breakage, the more negative of the stresses, σ_{xx}, in Figure 2 decreases slowly due to work hardening caused by the disappearance of the thinnest ice and the growth of pressure ridges. It is very important to note that the stresses in the discussion that follows were the ones calculated and averaged over the last 500 s of each simulation, when, as shown in Figure 2, the stresses have reached some semblance of steady state behavior, albeit slowly work-hardening due to ridge growth. It is important to emphasize that the stresses in the final 500 s do not reflect the initial uniformly frozen state of the model pack.

The off-diagonal stresses calculated using the first two methods discussed above, the boundary method and the internal method, were close to zero, while the off-diagonal stresses calculated using the boundary element method were similar in magnitude to the diagonal components. This shows that, while the *x* and *y*-direction stresses passing through the system are calculated properly by the boundary element method, the contact loads on the individual floes give rise to tensile and compressive forces within the floes. This results in a rotation of the principal stresses at points within the floes such that they are no longer aligned with the global *x,y* coordinate frame.

4. Stress in the Model Ice Pack

Simulations were run using a range of principal strains from uniform divergence through uniform convergence and back. The strain rate tensor $\dot{e}$ was comprised of the diagonal terms $\dot{e}_{xx}$ and $\dot{e}_{yy}$. The off diagonal terms were both zero. The magnitude of the rate of deformation, $\dot{e} = \sqrt{2}(\dot{e}_1^2 + \dot{e}_2^2)^{1/2}$, was held constant. The diagonal terms $\dot{e}_{xx}$ and $\dot{e}_{yy}$ were chosen by setting $\dot{e}_{xx} = \dot{e}\cos\theta$ and $\dot{e}_{yy} = \dot{e}\sin\theta$, varying θ from 0° to 360° in 7.5° increments. In the following discussion deformation is expressed in terms of the strain rate invariants $\dot{e}_I$ (the divergence of velocity) and $\dot{e}_{II}$ ($\pm 2(-\det \dot{e}')^{1/2}$) following *Rothrock* [1975].

Two sets of simulations were performed. In the first set the floes in the interior of the model pack were not 'frozen' together. That is, contacts between adjacent floes could not support tensile forces. In the second set of simulations the floes were initially 'frozen' together. The duration of each simulation was 5000 s. The model pack at the end of a simulation for the case of uniform divergence ($\dot{e}_I = 2\times10^{-6}$ s^{-1} and $\dot{e}_{II} = 0$), with the floes initially frozen together, is shown in Figure 1. The dark lines running through the model pack are leads. The parameters used in the simulations are listed in Table 1.

Table 1. Parameters Used in the Simulations.

Parameter	Symbol	Value
Strain rate magnitude	$\dot{e}$	2×10^{-6} s^{-1}
Pack width and height		90 km
Ice tensile strength	σ_t	600 kPa
Ice density	ρ_i	920 kg m^{-3}
Sea water density	ρ_w	1010 kg m^{-3}
Floe elastic contact stiffness	k_n	250 kN m^{-1}
Friction coefficient	μ	0.5
Water drag coefficient	C_w	0.005

The tensile strength σ_t used in the simulations was from *Richter-Menge and Jones* [1993]. Values of ρ_w, ρ_i, and C_w were from *Hibler* [1986]. The elastic contact stiffness k_n was chosen with an eye to computational efficiency, since the nominal time step is proportional to the square root of the minimum floe mass divided by the stiffness. The time step in the simulations was 1 s. The friction coefficient μ was chosen arbitrarily. It is the mid-range value tested by *Hopkins* [1996] and is meant to incorporate some of the effects of floe perimeter roughness. There were about 2000 floes in the model pack. The thickness distribution *g(h)* used to initialize the thin end of the thickness distribution of the individual floes is given in Table 2. Ice thicker than 2 m did not enter the ridging calculations because of the brevity of the simulations.

Table 2. Initial Ice Thickness Distribution.

h (m)	g(h) (m^{-1})	h (m)	g(h) (m^{-1})	h (m)	g(h) (m^{-1})
.125	.110	.875	.140	1.625	.170
.375	.119	1.125	.151	1.875	.170
.625	.128	1.375	.161	2.125	.169

During each simulation the energy balance was calculated to verify the self-consistency of the simulation. The components of the energy balance are boundary work, inelastic dissipation (including ridge building), frictional dissipation, and water drag. The calculations are described in *Hopkins* [1996]. The error in the energy balance was less than 1% of the total work performed by the boundaries.

The stresses that were calculated in both sets of simulations by the internal method (2) were plotted on principal stress axes to define a yield surface. The yield surface for the unfrozen pack is shown in Figure 3. The data points represent the average of the stresses over the last 500 s of each simulation. The strain vector corresponding to each data point is shown by the attached arrow. The general shape of the yield surface could be described as a tear drop. This shape was obtained by *Hopkins* [1996] in simulations with a similar, but more detailed, granular model of the ice pack, which was also unfrozen. This is also one of the yield curves obtained analytically by *Rothrock* [1975]. The strain vectors show that, except at points in the compressive region, the normal flow rule is not obeyed. Another point which may be noted is that the data points are fairly evenly spaced around the yield surface.

The yield surface for the frozen pack is shown in Figure 4. The stresses, calculated by the internal method (2), from 3 simulations using 3 different initial configurations were

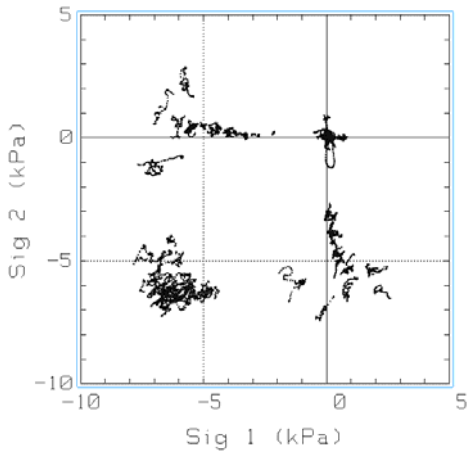

Figure 5. Yield surface constructed from the results of simulations with a frozen model pack. The data points are stresses averaged over 10 s intervals during the final 500 s of the simulations.

strain vector associated with the stress data points.

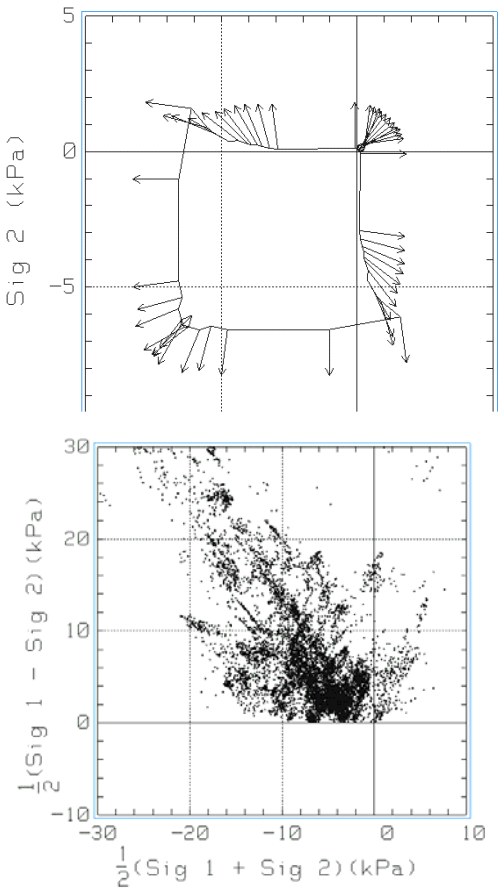

Figure 6. Boundary element principal stresses from a simulation with a frozen pack for a state of uniform convergence.

averaged together to obtain each data point. Since the data is not as smooth I have averaged the data about the line of symmetry. Again, the data points represent the average of the stresses over the last 500 s of each simulation. The strain vector corresponding to each data point is shown by the attached arrow. The general diamond shape of the yield surface was the one chosen for the AIDJEX constitutive law by *Pritchard* [1981]. A similar yield surface has been deduced from field measurements by [Co*on, et al*. 1998]. The normal flow rule seems to apply except in the region around pure shear ($\dot{e}_{\mathrm{I}} = 0$ and $\dot{e}_{\mathrm{II}}=2\times10^{-6}\mathrm{s}^{-1}$). Interestingly, in contrast to the unfrozen state in Figure 3, the data points congregate around states of uniform divergence, pure shear, and uniform convergence. In particular, strains having no convergent components congregate around a state of uniform divergence; strains having no divergent components congregate around a state of uniform convergence; strains having one divergent and one convergent component congregate around a state of pure shear. This congregation of the data points into distinct regions is clearly shown in Figure 5. The individual data points obtained at 10 s intervals over the last 500 s of each simulation are plotted. The data has not been averaged about the line of symmetry. The concavity of the yield surface in Figure 4 may be due to the small size of the model ice pack and the small number of slip lines that develop in it (see Figure 8).

Principal stresses calculated by the boundary element method from a simulation in which the strain invariants $\dot{e}_{\mathrm{I}} = -2\times10^{-6}\ \mathrm{s}^{-1}$ and $\dot{e}_{\mathrm{II}} = 0$ (ie. uniform convergence) are plotted in Figure 6. The pressure invariant (half the sum of the principal stresses) is plotted on the horizontal axis and the shear invariant (half the difference) is plotted on the vertical axis. In this simulation the floes were initially frozen together. The stresses were calculated at the center of 100 randomly chosen floes at 10 s intervals during the final 500 s of the simulation. Table 3 lists the average principal stresses calculated using the boundary stress method (I) and the boundary element method (III) for 3 deformation states; pure shear, uniaxial convergence and uniform convergence. The stresses for both methods were averaged over the final 500 s of the simulations. Table 4 lists the pressure-resultant invariant and shear-resultant invariant calculated using methods I and III for the same deformation states.

Table 3. Principal stress comparison.

$\dot{e}_{\mathrm{I}}$	$\dot{e}_{\mathrm{II}}$	σ_1 I	σ_2 I	σ_1 III	σ_2 III
$10^{-6}\ \mathrm{s}^{-1}$	$10^{-6}\ \mathrm{s}^{-1}$	kPa	kPa	kPa	kPa

0	2	0.28	-4.03	3.08	-7.07
-1.414	-1.414	-1.02	-6.57	4.14	-11.25
-2	0	-6.04	-6.08	0.76	-15.24

Table 4. Principal stress sum and difference comparison.

$\dot{e}_{\mathrm{I}}$	$\dot{e}_{\mathrm{II}}$	$\frac{1}{2}(\sigma_1+\sigma_2)$ I	$\frac{1}{2}(\sigma_1+\sigma_2)$ III	$\frac{1}{2}(\sigma_1-\sigma_2)$ I	$\frac{1}{2}(\sigma_1-\sigma_2)$ III
10^{-6} s^{-1}	10^{-6} s^{-1}	kPa	kPa	kPa	kPa
0	2	-1.88	-1.99	2.16	5.07
-1.414	-1.414	-3.79	-3.56	2.78	7.70
-2	0	-6.06	-7.24	0.02	8.00

The pressure-resultant invariants are quite similar. The difference is probably due to the relatively small number (100) of boundary element stress sites. The shear-resultant invariants are very different. This difference is probably due to the fact that the individual floes (represented in the boundary element model as linear elastic continua) have a higher tensile strength (in this case infinite) than the discontinuous model ice pack composed of discrete floes.

The amount of lead area and ridged ice area at the end of each simulation in the second set is shown in Figure 7 as a function of θ defined as $\theta=\tan^{-1}(\dot{e}_{II}/\dot{e}_{I})$ by *Rothrock* [1975]. A value of θ equal to zero corresponds to uniform divergence and a value of θ equal to π corresponds to uniform convergence. Net opening and ridging are expressed as a percentage of the area of the entire domain. The net shear and divergence are also shown in Figure 7. The duration of each simulation was 5000 s. In the simulations the

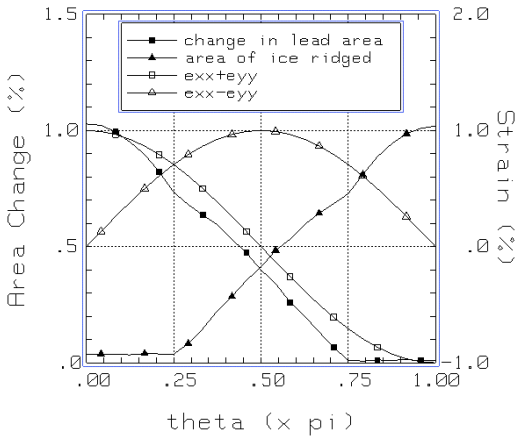

Figure 7. Area of leads and ridged ice as a fraction of total area at the end of each simulation as a function of θ. Net shear and divergence are also shown as a function of θ. Results of simulations with a frozen pack.

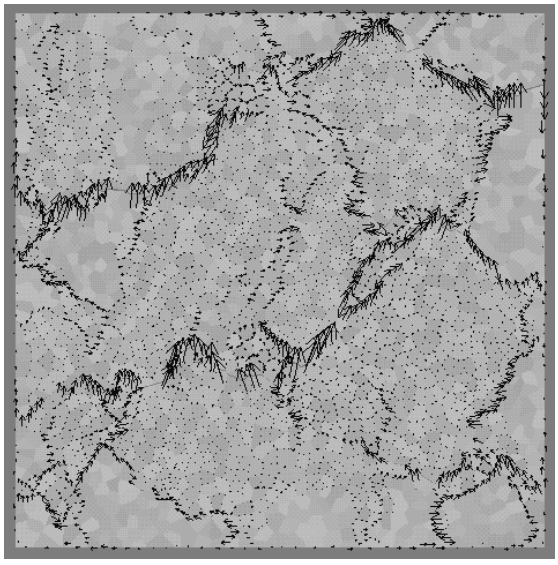

Figure 8. Model ice pack after undergoing pure shear deformation ($\dot{e}_{I} = 0$ and $\dot{e}_{II} = 2\times10^{-6}$ s^{-1}). The floes were initially frozen together. The small vectors show relative motion between adjacent floes.

simulations the floes were initially frozen together. The opening and ridging are nearly mirror images of each other and both follow the net divergence curve quite closely.

The profound difference in the yield curves in Figures 3 and 4 is due to the presence or absence of tensile strength in the model ice packs used in the two sets of simulations. Tensile strength also produces a similarly large effect in the deformation in the two cases. The deformation of the frozen pack for a state of pure shear is shown in Figure 8. The small vectors in the figure are proportional to the change in the line of center vectors between neighboring floes. The figure shows that the deformation is concentrated along the boundaries of large aggregates of floes with relative motion occuring both normal and parallel to the boundaries. The deformation state of the unfrozen pack for the same state of pure shear shows nearly uniform distribution of relative motion vectors. The stark difference between the two patterns of deformation must be responsible for the difference in the yield surfaces.

5. Conclusions

A granular model of the Arctic ice pack was used to simulate a range of deformation states from uniform convergence to uniform divergence. Two sets of simulations were performed. In the first set the floes that make up the model pack were in an unfrozen state, that is, the joints between adjacent floes were not able to support tensile forces. In the second set the floes were initially frozen together and the joints between adjacent floes were able to support tensile forces.

Stresses were calculated in the model ice pack in 3 ways: by dividing boundary forces by boundary lengths; using the contact forces between adjacent floes; and by using a boundary element technique to calculate the internal stresses at the centers of 100 of the nearly 2000 floes. The x and y direction stresses calculated with the 3 methods showed good agreement. With the first two methods, the pricipal stress directions were closely aligned with the principal strain directions (x and y) and the off diagonal terms of the two stress tensors were nearly zero. However, the principal stress directions calculated with the boundary element method in the interior of the floes were widely scattered as were the magnitudes. The pressure-resultant invariants for the 3 methods were quite similar. The difference was probably due to the relatively small number of boundary element stress sites. However, the shear-resultant invariants were very different. This difference is probably due to the fact that the individual floes (represented in the boundary element model as linear elastic continua) have a higher tensile strength (in this case infinite) than the discontinuous model

ice pack composed of discrete floes that can separate to form leads. Also, the lack of failure mechanisms at the floe scale such as the presence of thermal cracks or other flaws that might relieve tensile stress probably causes the boundary element method to overestimate the tensile stress within floes.

The stresses calculated in the two sets of simulations were plotted on principal stress axes to form yield curves. The yield curves were strikingly different. In the unfrozen case the yield curve was a rather perfect tear drop shape, while in the frozen case the yield curve was an untidy diamond-shaped surface. Not only were the shapes very different, but the distribution of the 48 individual deformation states about the yield curves were rather uniform in the unfrozen case and strongly clustered in the frozen case. The marked qualitative difference between the two yield curves was related to an equally marked qualitative difference between the deformation patterns created during the two sets of simulations. In simulations with the frozen pack, deformation occured along the boundaries of large aggregates of floes. While in simulations with the unfrozen pack, deformation was uniformly spread over the entire domain.

The low overall stress levels in the simulations were due to the large amount of thin ice in the initial thickness distribution and the fact that the thin ice was distributed uniformly over all of the floes. This gave the model pack a uniformity it would not normally have in a long-term simulation driven by realistic non-uniform derformation fields and subject to thermodynamic ice growth and melt. The resulting non-uniformity in the ice thickness distribution would be expected to cause a seasonal fluctuation in overall average stress levels.

Acknowledgments

This work was supported by funding from the NASA Mission to Planet Earth (97-MTPE-06) and the NSF Office of Polar Programs (OPP 9702040A).

References

Brebbia, C.A., and J. Dominguez, 1992. Boundary Elements, An Introductory Course, WIT Press/Computational Mechanics Publications, Boston.

Coon, M.D., G.S. Knoke, D.C. Echert, and R.S. Pritchard, 1998. The architecture of an anisotropic elastic-plastic sea ice mechanics constitutive law, *J. Geophys. Res*., 103, 21915-21925.

Cundall, P.A., and O.D.L. Strack, 1979. A discrete numerical model for granular assemblies, *Geotechnique*, 29, 47-65.

Hibler, W.D., III, 1986. Ice dynamics, in *The Geophysics of Sea Ice*, edited by N. Untersteiner, 577-640, Plenum, New York.

Hopkins, M.A., 1996. On the mesoscale interaction of lead ice and floes, *J. Geophys. Res*., 101, 18315-18326.

Hopkins, M.A., 1998. On the four stages of pressure ridging, *J. Geophys. Res.* 103, 21883-21891.

Kovacs, A., and D.S. Sodhi, 1980. Shore ice pile-up and ride-up: field observations, models, theoretical analyses, *Cold Reg. Sci. Tech.*, 2, 209-288.

Overland, J.E., McNutt, S.L., and S. Salo, 1998. Arctic sea ice as a granular plastic, *J. Geophys. Res.,* 103, 21845-21867.

Pritchard, R.S. 1981. Mechanical behavior of pack ice, in *Mechanics of Structured Media*, Part A, edited by A.P.S. Selvaduri, Elsevier, Amsterdam, 371-405.

Richter-Menge, J.A., and K.F. Jones, 1993. The tensile stress of first-year sea ice, *J. Glac.*, 39, 609-618.

Rothrock, D.A. 1975. The energetics of the plastic deformation of pack ice by ridging, *J. Geophys. Res.,* 80, 4514-4519.